

Mechanical performance of carbon-fibre braided composite tubes in tension and compression

4 Umair Javaid, Pierre Aumjaud, Barry Whelan and Philip
5 Cardiff

6 School of Mechanical and Materials Engineering, University
7 College Dublin, Ireland

8 November 22, 2021

Abstract

This article examines the effect of braid angle on the mechanical performance of carbon-epoxy braided tubes in tension and compression. Vacuum-assisted resin transfer moulding is used to produce a variety of tubes with several combinations of 15° and 20° braid angles. As uniaxial tensile testing of cylindrical tubes is not trivial, two tensile testing fixture designs are explored. It is found that a combination of mechanical and adhesive gripping produces repeatable fractures between the grips, with no slipping. Tubes with lower braid angles exhibit higher strengths both in tension and compression, as well as absorbing greater amounts of energy in compression.

20 **Keywords**

21 Biaxial braided tubes; carbon fibre composites; braid angle; grip design;
22 vacuum-assisted resin transfer moulding

23 1 Introduction

24 Braided composites consist of interwoven yarns embedded in a resin system
25 [1]. Thanks to their high strength-to-weight ratio and performance under 3-
26 D stress states, tubular braided composites are increasingly used in a variety
27 of applications, including biomedical [2], sports [3, 4], aerospace [5] and mil-
28 itary [6, 7]. In contrast to laminated composites, braided composites exhibit
29 greater impact resistance [8] and the opportunity to make near net shape
30 preforms. Recent studies have shown that carbon fibre braided tubes are ex-
31 cellent candidates for space applications structures due to their high specific
32 stiffness, thermal stability and superior fatigue resistance [9, 10]. In biaxial
33 tubular braiding, fibre strands/tows are intertwined around a tubular man-
34 drel in clockwise and counterclockwise directions, resulting in a bidirectional
35 helically interlaced structure (Figure 1) [11]. The helix angle with respect to
36 the tube axis is known as the braid (or braiding) angle and has theoretical
37 values between 0° and 90° . Due to manufacturing constraints, braid angles
38 range from 15° to 75° . A braid angle of 0° indicates a tow oriented axially
39 and not wrapped around the component, whereas 90° indicates a tow that
40 wraps around the structure but does not progress along the main axis, similar
41 to filament winding.

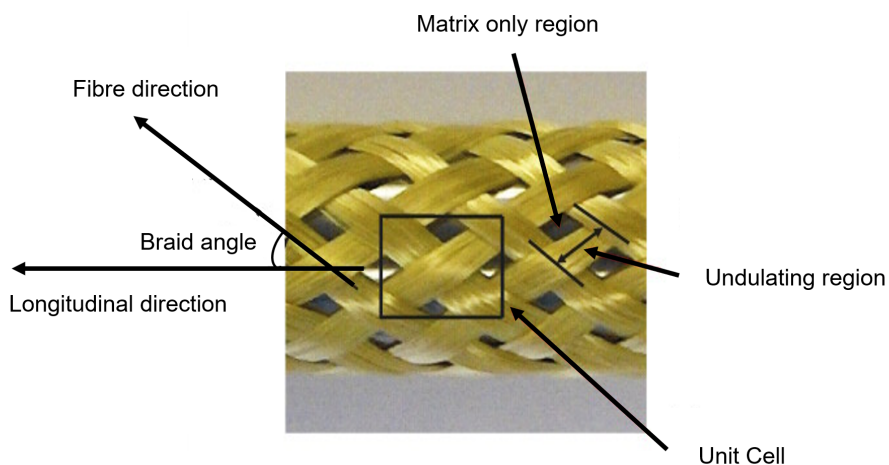


Figure 1: 2-D biaxial braids (adapted from [12]).

42 The braid angle greatly affects the mechanical properties of composite
43 braids, and many studies have examined its effect on the mechanical perfor-
44 mance of braided composites [13, 14, 15, 16, 17, 18, 19]. Previous studies have
45 established that an increase in braid angle is accompanied by a decrease in
46 tensile strength [20, 21], peak failure load [22, 23] and tensile modulus [23, 24],
47 and by an increase of axial failure strain [25] and stress wave propagation
48 speed [26].

49 Tensile testing of intact tubes is difficult for a number of reasons [27, 28]:
50 1) custom grips are required; and 2) specimen slipping is a common occur-
51 rence. As a result, much of the available literature on braided composites
52 focuses on testing of flat specimens [24, 29, 30, 31, 32, 33]. While this ap-
53 proach gives a good indication of the behaviour of braided tubes, it also
54 presents some drawbacks [34]:

- 55 ● *Edge effects*: premature failure can occur at the free edges of flat spec-
56 imens;
- 57 ● *Fibre relaxation*: braided fabrics lose some of their integrity and straight-
58 ness when cut;
- 59 ● *Void content and distribution*: the void content and its distribution in
60 flat specimens may differ from those in tubular specimens.

61 A number of approaches for gripping intact tubes during tensile testing
62 have been reported in the literature [35, 27, 13, 14, 15, 17, 18, 19]. The
63 most common design is a double mounting grip in which the braided tube is
64 clamped between inner and outer circular fixtures as shown in Figure 2.

65 This design is able to accommodate tubes of large diameters, however the
66 contact surface between tube and centre clamp is limited, which may result
67 in increased slipping. Moreover, this design does not offer much flexibility
68 on the tube geometry as it is restricted to tubes of uniform cross section and
69 fixed diameter. Any alteration in the design to accommodate different tube
70 geometries and sizes would be challenging to manufacture.

71 Perillo et al. proposed a customised grip design as shown in Figure 3.
72 This design allows the testing of tubes of various diameters; however the

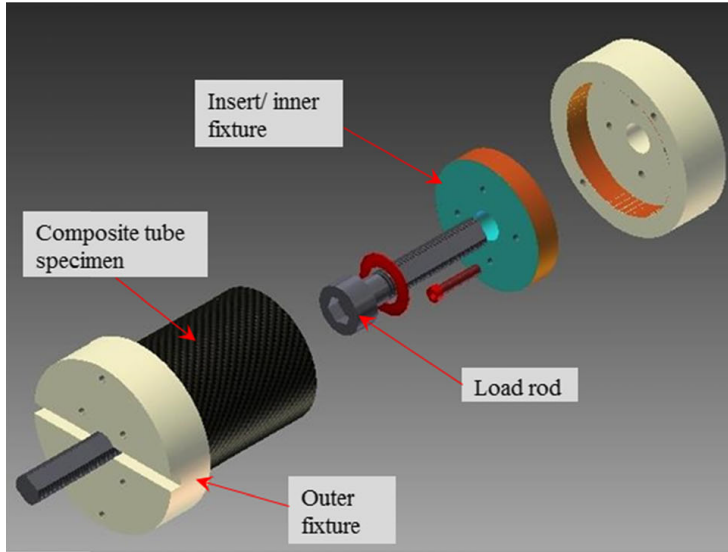


Figure 2: Existing approach for the tensile test of braided tubes (adapted from [27])

73 V-shaped clamping grip may result in increased local stress regions, which
 74 may induce cracking.

75 In the present article, we describe an alternative tensile testing procedure
 76 for tubular braided composite structures, as well as characterising braided
 77 tubes in tension and compression for a variety of braiding angles.

78 The remainder of this article is structured as follows: Section 2 describes
 79 the materials used and sample preparation steps. Section 3 describes the
 80 tensile and compression testing methods, as well as the design of a novel
 81 gripping procedure for full tube tensile tests. A finite element model of the
 82 tensile test is also reported. The results and discussion are given in Section
 83 4, and Section 5 briefly outlines the conclusions of the work.

84 2 Materials and Tube Fabrication

85 2.1 Materials

86 Two types of carbon fibre biaxial braided sleeves (15° and 20°) were pro-
 87 vided by Burgmann Packings Ltd [36]. Each sleeve is composed of approx-

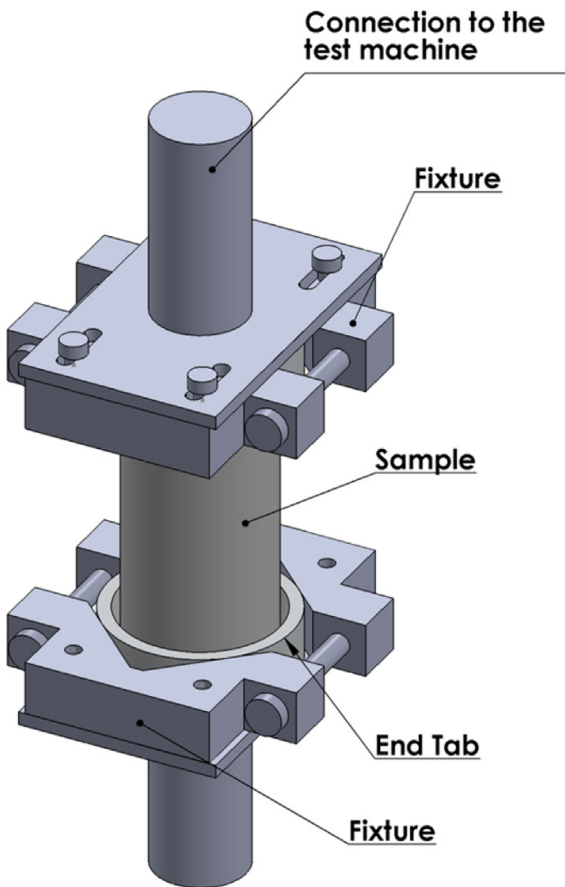


Figure 3: Custom grip design by Perillo et al. (adapted from [35])

88 imately 3000 yarns ($7 \mu\text{m}$ diameter) bundled into 128 individual threads;
89 these threads are braided together in a diamond pattern and oriented at an
90 angle of $\pm\theta$ with respect to the sleeve's axis. An IN2 Infusion epoxy resin
91 system was used with the AT30 slow curing agent (100:30 mixing ratio by
92 weight) [37].

93 2.2 Tube Fabrication

94 Each tube is manufactured with four layers of braided sleeves; the following
95 sleeve stacking sequences are examined (from the inside towards the outside
96 of the tube):



(a) Mould assembly

(b) Vacuum seals (in blue)

Figure 4: Mould used to manufacture the braided tubes.

97 • **BR-15:** $[\pm 15]_4$

98 • **BR-20/15:** $[\pm 20 / \pm 15]_2$

99 • **BR-20:** $[\pm 20]_4$

100 The tubes are infused in a two-part aluminium mould with a 25 mm
 101 diameter steel mandrel provided by Burgmann Packings Ltd [36] (Figure 4).
 102 The infusion process by Vacuum Assisted Resin Transfer Molding (VARTM)
 103 consists of the following steps (a schematic representation of the process is
 104 given in Figure 5):

- 105 1. The mandrel and mould cavity are coated with the Easy-Lease releasing
 agent [37] to facilitate demoulding;
 - 106 2. Four layers of braided sleeves are pulled over the mandrel, according
 to the chosen design (BR-20, BR-15 or BR-20/15);
 - 107 3. The mandrel wrapped with braided sleeves is placed in the cavity, and
 the mould is bolted closed. The mould is then placed in a vertical
 orientation with the inlet at the bottom and outlet at the top;
 - 108 4. The resin is preheated to 40°C and degassed. Subsequently, a vacuum
 pressure of -1 bar is applied to the mould causing the resin to infuse
 into the mould.
- 115 The infusion process takes 10 minutes;

- 116 5. Once the resin reaches the outlet, some extra resin is allowed to bleed
 117 out for a few minutes to remove air bubbles in the resin flow and the
 118 inlet and outlet gate valves are closed. The vacuum port is kept open
 119 until the remaining resin in the reservoir has cured. The tubes are then
 120 left to cure for 30 hours at room temperature;
- 121 6. Once the mould is opened, the tube is pushed off the mandrel from one
 122 end of the assembly while holding the cured tube firmly using a custom
 123 extraction tool;
- 124 7. The tubes are post-cured at 80°C for 2 hours;
- 125 8. The cured tubes are cut into segments of the required length with a
 126 band saw cutter.

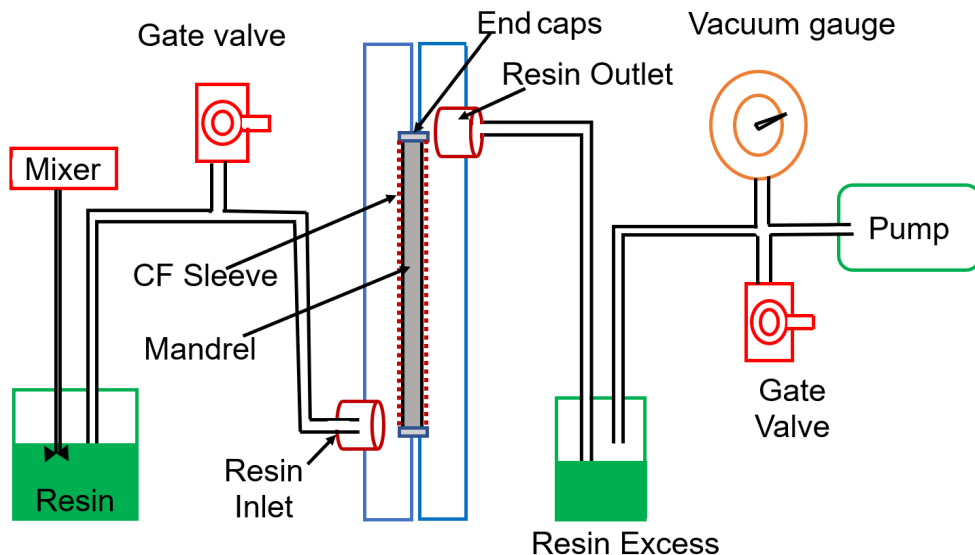


Figure 5: Infusion process setup.

127 The outer diameters and wall thicknesses of the tubes after curing are
 128 given in Table 1.

Braid configuration	Outer diameter (mm)	Wall thickness (mm)
BR-15	30.21 ± 0.05	2.60 ± 0.03
BR-20/15	30.14 ± 0.16	2.57 ± 0.08
BR-20	30.09 ± 0.06	2.54 ± 0.03

Table 1: Mean outer diameters and wall thicknesses after curing, with standard deviations.

129 3 Methods

130 3.1 Tensile Testing

131 The braided tubes are cut to a length of 150 mm and constrained in tension
 132 with a hydraulic Instron universal testing machine and a 250 kN load cell
 133 according to the ASTM D5450 standard [38]. The test apparatus can be seen
 134 in Figure 6. The tests are carried out with a constant crosshead displacement
 135 of 1.3 mm/min. The tubes are loaded to failure and the load and the failure
 136 displacements are recorded. The axial engineering stress within the tubes is
 137 calculated by dividing the load by the initial cross-sectional area. The failure
 138 strain is computed by dividing the displacement at failure by the distance
 139 between the grips (100 mm).

140 Each test is repeated three times. Given the tubular shape of the speci-
 141 mens as well as the loads involved, the design of a suitable gripping mecha-
 142 nism is critical to ensure repeatable testing. With this in mind, two separate
 143 gripping system designs are examined, as described in Section 3.3 below.

144 3.2 Compression Testing

145 Compression testing is performed according to the ASTM 695-02 [39] stan-
 146 dard, as shown in Figure 7. The specimens are cut to a height of 30 mm,
 147 yielding a unity height-to-diameter ratio. Once again, testing is performed
 148 on a hydraulic Instron universal testing machine with a 250 kN load cell. The
 149 specimens are compressed between two parallel smooth and flat steel plates

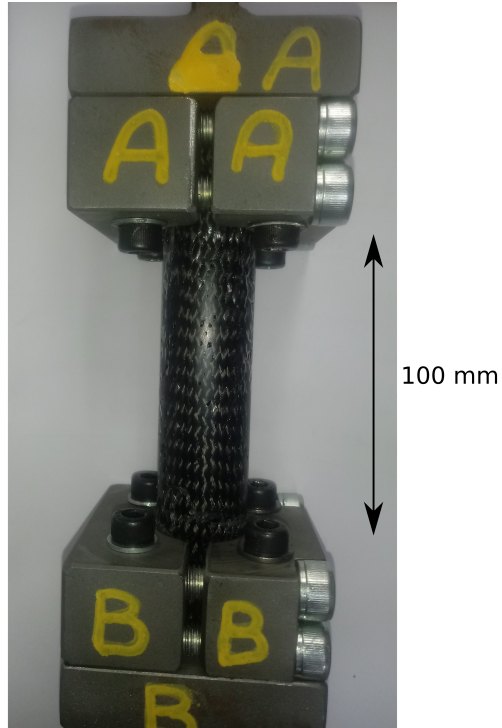


Figure 6: Experimental setup for the tensile test of braided tubes.

150 at a rate of 1.3 mm/min, and the force is recorded. In addition, the failure
 151 mechanism is noted. These tests are repeated thrice. For each tensile and
 152 compression test, the three following metrics are computed:

- 153 • The strength, defined as the first load peak divided by the undeformed
 154 cross-sectional area;
- 155 • The axial stiffness, defined as the strength divided by the strain at
 156 break.
- 157 • The energy density, defined as the area under the force–displacement
 158 curve per unit volume:

$$E_d = \frac{1}{V} \int_0^{l_{\max}} P(l) \, dl \quad (1)$$

159 where P is the load, l is the vertical displacement and V is the volume
160 of the specimen;

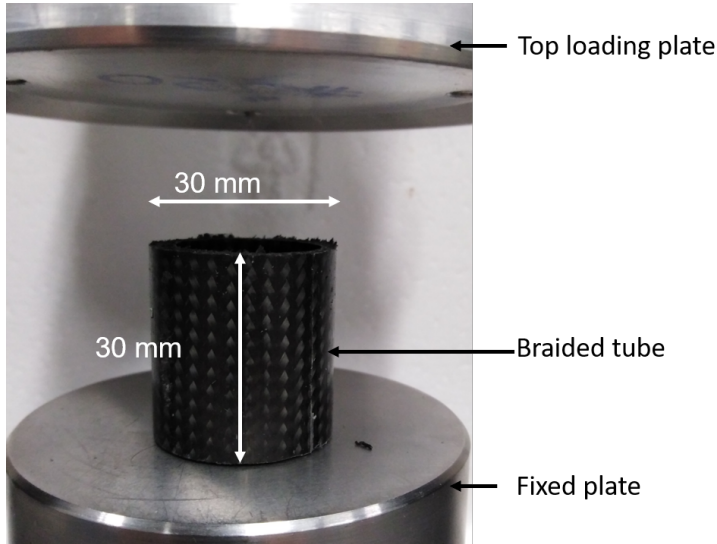


Figure 7: Experimental setup for the compression testing of braided tubes.

161 **3.3 Design of a Novel Gripping System for Tensile
162 Testing of Tubes**

163 Following the general specifications of the ASTM D5450 standard (tensile test
164 method for hoop-wound composite cylinders), two grips designs are proposed.

165 **3.3.1 Design I**

166 The first design (Figures 8 and 9) is based on an internal cup and cone placed
167 inside each end of the tube, which are then bolted to the external fixture of
168 the testing machine. This design has a much greater surface contact area as
169 compared to the designs proposed by Roy et al [27]. The external fixture
170 consists of a clamping disk/cylinder which fits around the end of the tube.
171 As the internal bolt is tightened, it pushes the internal cone against the
172 internal cup, causing mechanical gripping. The outer surface of the cup
173 is sand-blasted to increase its friction coefficient. The external clamping

174 disk/cylinder provides support against this internal pressure to avoid damage
 175 of the tube, as well as gripping the tube from the outside. As the bolt heads
 176 are within the tube, an internal alignment pin is inserted to allow tightening
 177 of the bolt at the other end. This alignment pin remains in place during
 178 testing but does not hold any force in tension. As the tensile test progresses,
 179 the increasing axial force on the internal bolts results in increasing gripping
 180 pressure applied by the cone via the internal cup.

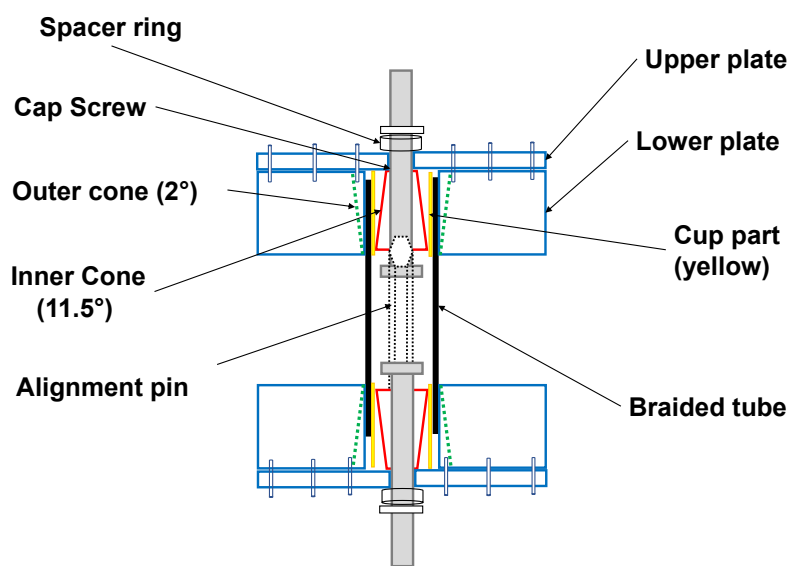


Figure 8: Design I grip schematics.

181 This design is an elegant gripping approach that does not require the
 182 use of any adhesive. However after several tensile test trials, the following
 183 limitations are noted:

- 184 • Significant machining time is required to produce the internal cup and
 185 cones components. In addition, a number of cone angles needed to be
 186 considered to yield a design that does not slip.
- 187 • The strength of the internal bolts provides an upper limit on the force
 188 supported by the grips, where the maximum bolt size that can be used
 189 is limited by the internal diameter of the tubes to be tested. One must

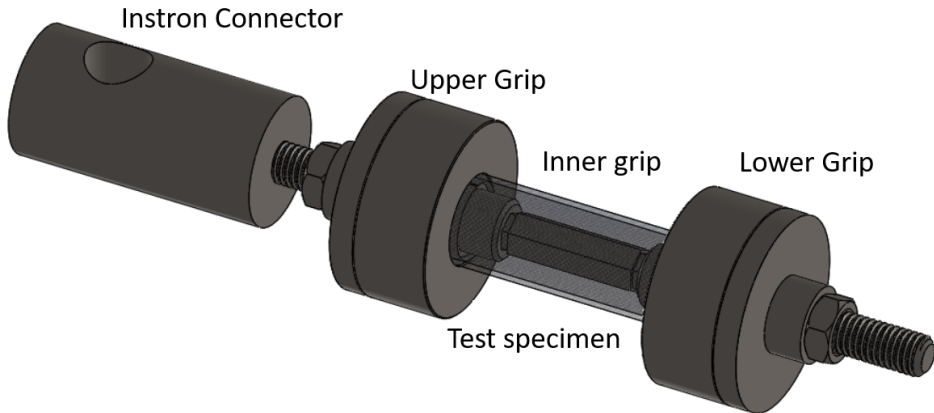


Figure 9: Design I grip assembly.

190 ensure that the largest bolt that fits inside the tubes is strong enough
 191 to perform the test;

- 192 • Many times during testing, the tubes starts to slip inside the grips,
 193 thus invalidating the tests.

194 3.3.2 Design II

195 The second design consists of a T-shaped mild steel section with a central
 196 protruding column, as shown in Figures 10, 11 and 15. The protruding
 197 column is inserted into the end of the tube and a pair of external side fixtures
 198 are simultaneously clamped to each other (M10 bolts) as well as to the T-
 199 shaped section (M8 bolts).

200 This design allows the external side fixtures to mechanically grip onto the
 201 tube. Initial testing found that this setup is able to successfully perform ten-
 202 sile testing on braided tubes, however intermittent slipping is still an issue.
 203 To overcome this, experimental grade fast-curing adhesive [40], supplied by
 204 Henkel Ireland, is applied to the T-shaped section and the inner side of the
 205 tube. The adhesive is cured at 110°C for 15 minutes. Through the combi-
 206 nation of mechanical and adhesive gripping, this gripper design eliminates
 207 slipping during testing. There are however a number of limitations with this

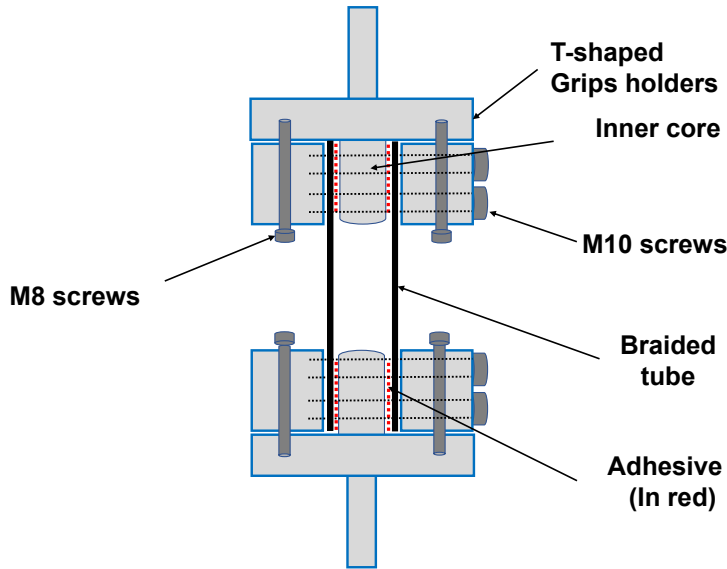


Figure 10: Design II grip schematics.

208 design:

- 209 • In order to avoid premature failure of the braided tubes at the grips,
210 the external side bolts should not be over-tightened. Through trial-
211 and-error, this value was found to be to 90 Nm for the current setup;
- 212 • As adhesive from previous tests must be removed between each test,
213 multiple gripping fixtures must be manufactured. Alternatively, only
214 one tube can be tested at a time.

215 Nevertheless, this approach is found to be sufficient robust and is used
216 for tensile testing.

217 **3.4 Finite Element Model**

218 The tensile testing of has been modelled in finite element software Abaqus
219 [41] in order to compare the trends observed experimentally. The braided
220 tubes are modelled as a quarter cylinder with length 100 mm and a diameter
221 corresponding to the configuration modelled (approximately 30 mm, see Ta-
222 ble 1). Symmetrical boundary conditions are imposed on the two long free

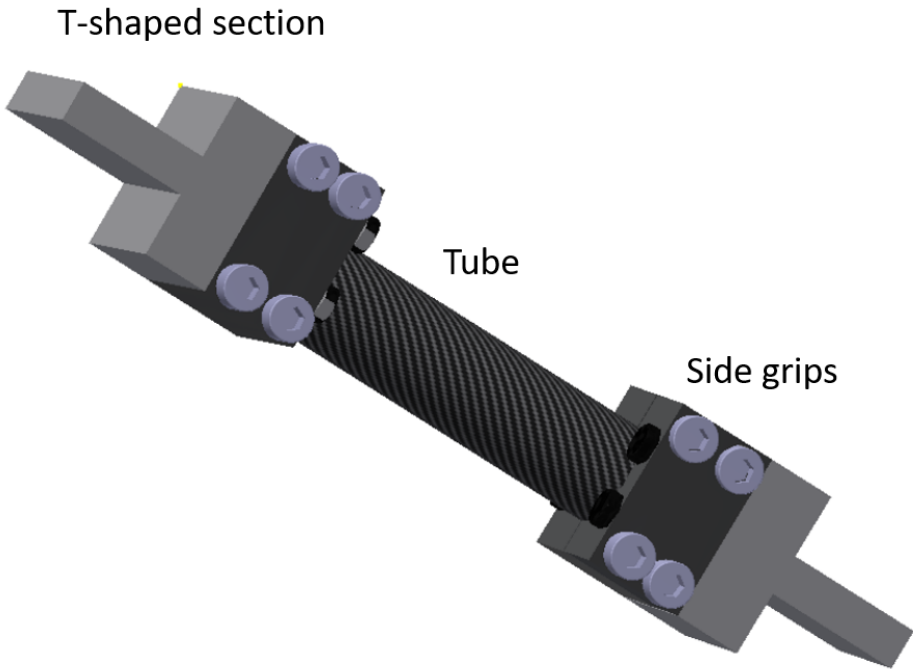


Figure 11: Design II grip assembly.

223 edges. A fully constrained boundary condition is applied to the edge at $z =$
 224 0 and a vertical upward displacement of 3 mm is imposed on the opposite
 225 edge. The model is meshed with 2200 S4R elements, which are 4-noded shell
 226 elements based on the first-order shear theory, featuring reduced integration,
 227 a large-strain formulation and hourglass control.

228 Each braided sleeve is modelled as a laminated composite layup of 2
 229 orthotropic plies whose fibres are oriented at an angle of $\pm\theta$ from the tube
 230 axis. This modelling choice is adopted to represent the braiding as a uniform
 231 component without having to model its microstructure. The ply thickness
 232 is defined as the tube wall thickness divided by the number of plies. For
 233 example, the BR-20/15 tube is composed of 8 plies of thickness 2.57/8 mm
 234 (approximately 0.3 mm) with the following ply orientation sequence: $[+20/-$
 235 $20/+15/-15]_2$. The material properties of the carbon-epoxy material are
 236 given in Table 2. These values are fitted to the experimental stress-strain
 237 curves shown in the result section and are comparable to those reported by

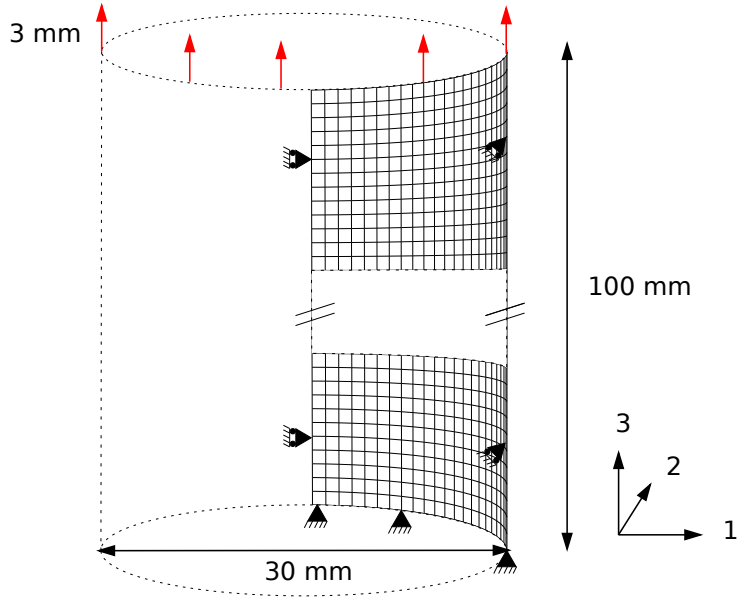


Figure 12: Mesh and dimensions of the finite element model.

238 Shi et al. [42].

239 At each time step, the vertical reaction force of the nodes at the top
 240 short edge of the tube is summed and recorded, together with its associated
 241 vertical displacement. The Hashin criterion is used to model damage in the
 242 composite and the model parameters are reported in Table 2.

243 4 Results and Discussion

244 4.1 Tensile Testing

245 The stress-strain curves of all tension sample are shown under tensile load is
 246 shown in Figure 13, both from experimental testing and finite element anal-
 247 ysis. All tests exhibit an approximately linear region followed by a sudden
 248 brittle failure, accompanied by a loud sound. The failure is sudden with al-
 249 most no observable damage prior to fracture. It can be seen that the strength
 250 and stiffness of the BR-15 sample (i.e. the tube with the lowest average braid
 251 angle) is the highest, followed by the BR-20/15 and BR-20 samples. Simi-
 252 lar trends are observed in finite element analysis. These results agree with

Material property	value
Longitudinal elastic modulus - E_1^0	87 GPa
Transverse elastic modulus - $E_2^0 = E_3^0$	10.3 GPa
Longitudinal shear modulus - $G_{12}^0 = G_{13}^0$	6 GPa
Transverse shear modulus - G_{23}^0	3.7 GPa
Longitudinal Poisson's ratio - $\nu_{12} = \nu_{13}$	0.3
Transverse Poisson's ratio - ν_{23}	0.4
Tensile strength in the fibre direction - X^T	3000 MPa
Compressive strength in the fibre direction - X^C	2370 MPa
Tensile strength perpendicular to fibre direction - Y^T	123 MPa
Compressive strength perpendicular to fibre direction - Y^C	354 MPa
Longitudinal shear strength - S^L	202.5 MPa
Transverse shear strength - S^L	90 MPa
Fracture energy dissipated in fibre tension - G_{ft}^C	9160 J/m ²
Fracture energy dissipated in fibre compression - G_{fc}^C	7990 J/m ²
Fracture energy dissipated in matrix tension - G_{mt}^C	2200 J/m ²
Fracture energy dissipated in matrix compression - G_{mc}^C	1100 J/m ²
Viscosity coefficients - $\eta_{ft} = \eta_{fc} = \eta_{mt} = \eta_{mc}$	0.001

Table 2: Material properties of the carbon-epoxy material.

253 the theory and literature: the tubes with fibres most aligned in the axial
 254 direction are stronger and stiffer [21, 23].

255 Examining the failure modes in Table 4, it can be seen that failure is
 256 due to a combination of fibre breakage and matrix cracking. In all samples,
 257 failure occurs between the two grips and not at the gripping location. This
 258 suggests that the gripping fixtures are effective at constraining the sample in
 259 tension without causing any excessive damage while gripping the sample.

260 4.2 Compression Testing

261 In compression, all tubes behave elastically up to an initial peak followed by
 262 a drop in load, corresponding to crack initiation and propagation, see Figure
 263 14. As the displacement increases, the stress continues to decline slowly
 264 while the tube is being crushed. Similar to the tensile tests, the tubes with
 265 the lowest braid angle (BR-15) shows the highest strength, while the BR-

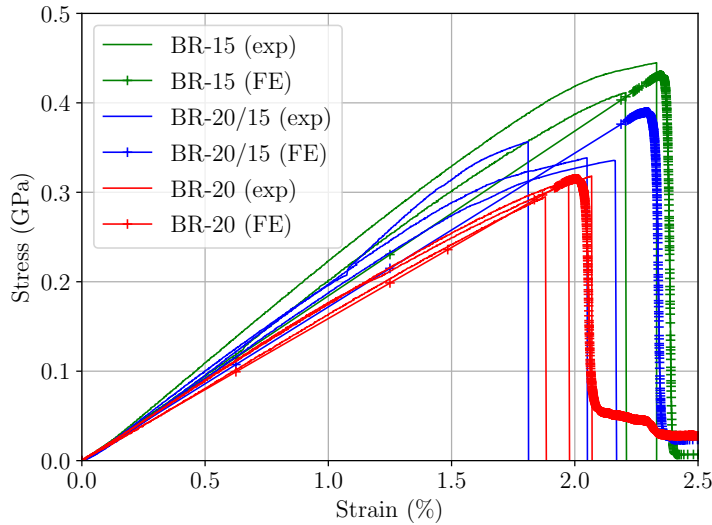


Figure 13: Stress strain curves of the three tube configurations obtained both from experiments and finite element analysis.

266 20/15 and BR-20 configurations exhibit comparable strengths. As crushing
 267 progressed, the stress carried by the BR-20/15 tube reduces at a slower rate
 268 than the other tubes, meaning that more energy is absorbed by the BR-20/15
 269 tube at comparable strength. This suggests that alternating plies with low
 270 and high fibre angles contribute to increasing the energy absorption capacity
 271 of braided tubes in compression.

272 The failure modes of the samples under a 9 mm compressive displacement
 273 are characterised by a combination of matrix cracking, fibre breakage and
 274 interply delamination, see Table 4.

275 The stiffness, strength and energy density of all the braided tube config-
 276 urations are compared in Table 3. Overall, the tube with the lowest braid
 277 angle (BR-15) exhibit the best mechanical performance in terms of stiffness,
 278 strength and energy density, both in tension and in compression. This is in
 279 agreement with the results found in the literature, suggesting that the grip-
 280 ping methodology adopted here is robust. Furthermore, the braided tube
 281 configurations considered here perform significantly better in tension than in
 282 compression. On average, the braided tubes in tension are stiffer, stronger
 283 and absorb more energy than the same tubes loaded in compression.

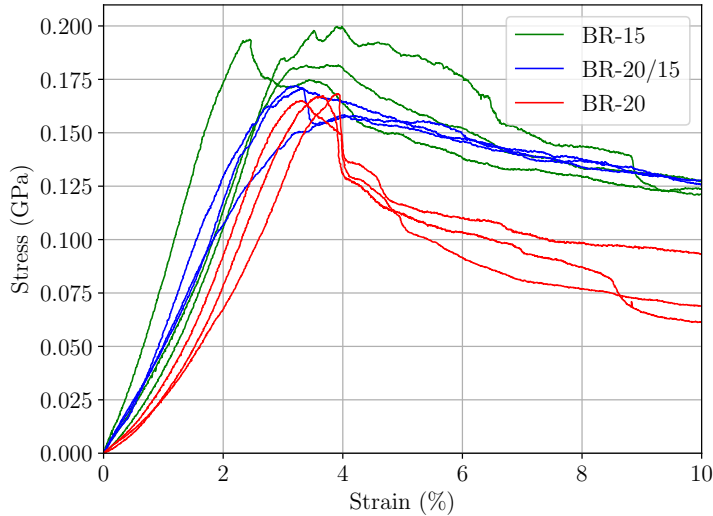


Figure 14: Stress-strain curve of the braided tubes under compressive loading.

284 5 Conclusion

285 In this study, the experimental characterisation of composite braided tubes
 286 under axial tensile and compressive loads is carried out. For tensile test-
 287 ing of full tubes, a new gripping design is proposed that successfully avoids
 288 slipping and premature fracture. It is found that the braiding angle has a
 289 significant effect on the ultimate tensile and compressive strengths. In tensile
 290 testing, the load-carrying capacity of the BR-15 configuration is found to be
 291 24% and 38% higher than that of the BR-20/15 and BR-20 configurations,
 292 respectively. In compression testing, the peak load, compressive strength
 293 and energy absorption capabilities are reported for comparison. It is found
 294 that the BR-15 configuration showed the highest crushing load compared to
 295 the BR-20 and BR-20/15 configurations. The BR-15 tube absorbed 24% and
 296 6.7% more energy than the BR-20/15 and BR-20 configurations, respectively.

297 6 Acknowledgements

298 Financial support is gratefully acknowledged from the Irish Composites Cen-
 299 tre (IComp), as well as technical assistance and advice from Alojz Ivankovic,

Test configuration	Stiffness (MPa)	Strength (MPa)	Energy density (KJ/m ³)
BR-15 - tension - exp	188.6 ± 2.2	427.9 ± 16.9	5125 ± 452
BR-20/15 - tension - exp	172.5 ± 17.6	343.5 ± 9.2	3854 ± 434
BR-20 - tension - exp	156.4 ± 1.9	308.7 ± 10.0	3361 ± 276
BR-15 - tension - FE	309.1	486.1	4959
BR-20/15 - tension - FE	282.3	450.4	4516
BR-20 - tension - FE	253.5	429.5	3290
BR-15 - compression - exp	-	191.8 ± 7.5	3617 ± 917
BR-20/15 - compression - exp	-	167.1 ± 6.1	3389 ± 502
BR-20 - compression - exp	-	166.9 ± 1.3	2911 ± 258

Table 3: Stiffnesses, strengths and energy densities of all tube configurations in compression and tension.

300 Michael Donohue, John Gahan and Tatiana Stefanov from University College
 301 Dublin. Materials are provided by Greg Byrne at Burgmann Packings Ltd.

302 **7 Declarations**

303 **7.1 Ethics approval and consent to participate**

304 Not applicable.

305 **7.2 Adherence to national and international regula-** 306 **tions**

307 Not applicable.

308 **7.3 Consent for publication**

309 Not applicable

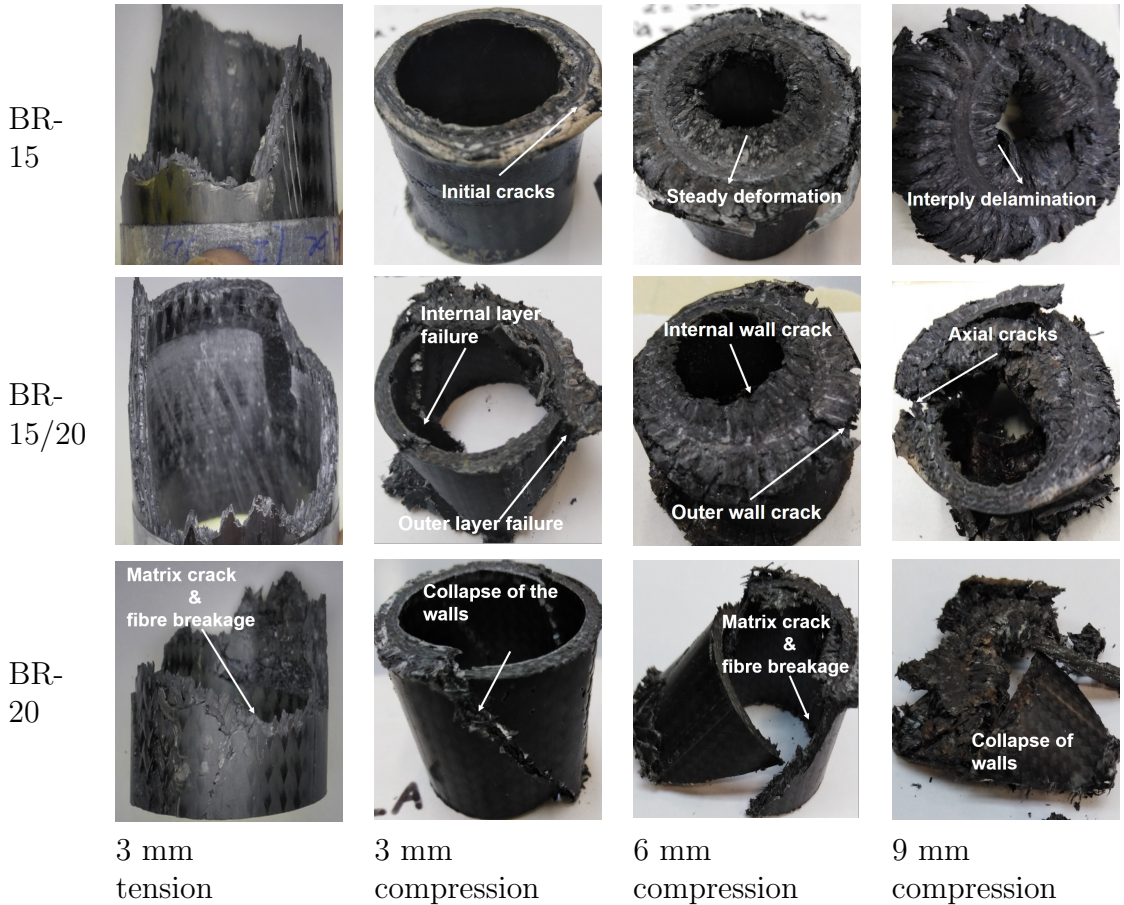


Table 4: Failure modes of the braided tubes in tension and compression.

310 7.4 Availability of data and material

311 Raw data were generated at University College Dublin. Derived data sup-
 312 porting the findings of this study are available from the corresponding author,
 313 PC, on request.

314 7.5 Competing interests

315 The authors declare that they have no competing interests.

316 **7.6 Funding**

317 Financial support is gratefully acknowledged from the Irish Composites Cen-
318 tre (IComp), which is jointly funded by Enterprise Ireland and IDA Ireland.

319 **7.7 Authors' contributions**

320 Conceptualisation, P.C. and U.J. and P.A.; methodology, P.C. and U.J. and
321 P.A.; software, P.C. and P.A.; writing—original draft preparation, U.J.;
322 writing—review and editing, P.C. and U.J. and P.A.; supervision, P.C.;
323 project administration, P.C.; funding acquisition, P.C.

324 **7.8 Acknowledgements**

325 Technical assistance and advice are gratefully acknowledged from Alojz Ivankovic,
326 Michael Donohue, John Gahan and Tatiana Stefanov from University College
327 Dublin. Materials are provided by Greg Byrne at Burgmann Packings Ltd.

328 **References**

- 329 [1] G.W. Melenka, A.J. Hunt, J.H. van Ravenhorst, R. Akkerman, C.M.
330 Pastore, F.K. Ko, M. Munro, and J.P. Carey. Manufacturing processes
331 for braided composite materials. In Jason P. Carey, editor, *Handbook of*
332 *Advances in Braided Composite Materials*, pages 47 – 153. Woodhead
333 Publishing, 2017.
- 334 [2] J.P. Carey. Introduction to braided composites. In Jason P. Carey,
335 editor, *Handbook of Advances in Braided Composite Materials*, pages 1
336 – 21. Woodhead Publishing, 2017.
- 337 [3] R. Parimala and D.B. Jabaraj. A study on nanophased biaxial car-
338 bon braided composites”, journal = ”Materials Today: Proceedings.
339 3(6):2268 – 2277, 2016. Recent Advances In Nano Science And Technol-
340 ogy 2015.

- 341 [4] Dodd H. Grande, Steve Greist, Tyler Jessie, and Jason Daniel. Com-
342 posites in Sports Applications. In Peter W.R. Beaumont and Carl H.
343 Zweben, editors, *Comprehensive Composite Materials II*, pages 469 –
344 526. Elsevier, Oxford, 2018.
- 345 [5] J.P. Carey, G.W. Melenka, A. Hunt, B. Cheung, M. Ivey, and
346 C. Ayrancı. Braided composites in aerospace engineering. In Sohel
347 Rana and Raul Fangueiro, editors, *Advanced Composite Materials for*
348 *Aerospace Engineering*, pages 175 – 212. Woodhead Publishing, 2016.
- 349 [6] M. Bulat, H. Ahlborn, F. Gnädinger, and D. Michaelis. Braided car-
350 bon fiber composites. In Yordan Kyosev, editor, *Advances in Braiding*
351 *Technology*, Woodhead Publishing Series in Textiles, pages 383 – 394.
352 Woodhead Publishing, 2016.
- 353 [7] Linhui Gong, Xuhao Gao, Heng Yang, Yinghua Liu, and Xuefeng Yao.
354 Design on the driveshaft of 3D 4-Directional carbon fiber braided com-
355 posites. *Composite Structures*, 203:466 – 473, 2018.
- 356 [8] Haili Zhou, Chao Li, Liquan Zhang, Bryn Crawford, Abbas S. Milani,
357 and Frank K. Ko. Micro-XCT analysis of damage mechanisms in 3D
358 circular braided composite tubes under transverse impact. *Composites*
359 *Science and Technology*, 155:91 – 99, 2018.
- 360 [9] C. Wu and A. Viquerat. Natural frequency optimization of braided
361 bistable carbon/epoxy tubes: Analysis of braid angles and stacking se-
362 quences. *Composite Structures*, 159:528 – 537, 2017.
- 363 [10] Y. Liu, M. de Araujo, and H. Hu. Advanced fibrous architectures for
364 composites in aerospace engineering. In Sohel Rana and Raul Fangueiro,
365 editors, *Advanced Composite Materials for Aerospace Engineering*, pages
366 17 – 58. Woodhead Publishing, 2016.
- 367 [11] Garrett W. Melenka, Eric Lepp, Benjamin K.O. Cheung, and Jason P.
368 Carey. Micro-computed tomography analysis of tubular braided com-
369 posites. *Composite Structures*, 131:384 – 396, 2015.

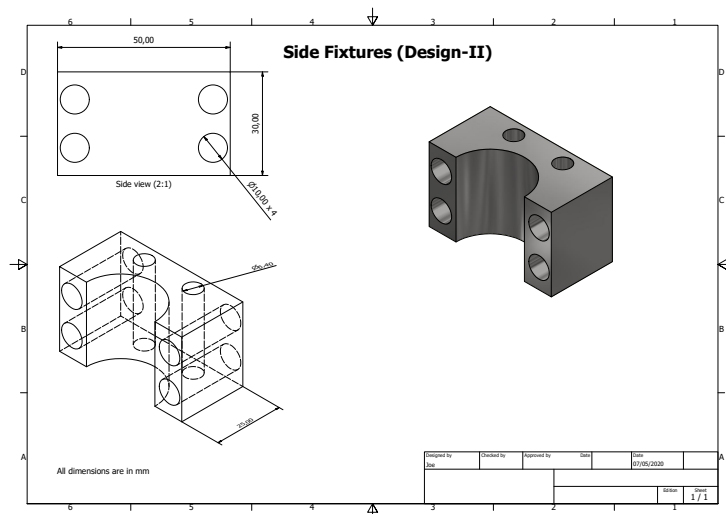
- 370 [12] Cagri Ayranci and Jason Carey. 2D braided composites: A review for
371 stiffness critical applications. *Composite Structures*, 85(1):43 – 58, 2008.
- 372 [13] Cagri Ayranci Jason P. Carey. Experimental validation of a regression-
373 based predictive model for elastic constants of open mesh tubular
374 diamond-braid composites. *Polymer Composites*, 32(2):243–251, 2010.
- 375 [14] Xinran Xiao, Hamid G. Kia, and Xiao Jing Gong. Strength prediction
376 of a triaxially braided composite. *Composites Part A: Applied Science
377 and Manufacturing*, 42(8):1000–1006, 2011.
- 378 [15] Lee W. Kohlman, Justin L. Bail, Gary D. Roberts, Jonathan A. Salem,
379 Richard E. Martin, and Wieslaw K. Binienda. A notched coupon ap-
380 proach for tensile testing of braided composites. *Composites Part A:
381 Applied Science and Manufacturing*, 43(10):1680–1688, 2012.
- 382 [16] Lei Xu, Seong Jong Kim, Cheng Huat Ong, and Sung Kyu Ha. Prediction
383 of material properties of biaxial and triaxial braided textile com-
384 posites. *Journal of Composite Materials*, 46(18):2255–2270, 2012.
- 385 [17] Lei Xu, Cheng Zhu Jin, and Sung Kyu Ha. Ultimate strength prediction
386 of braided textile composites using a multi-scale approach. *Journal of
387 Composite Materials*, 49(4):477–494, 2015.
- 388 [18] T. D. Vu, D. Durville, and P. Davies. Finite element simulation of
389 the mechanical behavior of synthetic braided ropes and validation on a
390 tensile test. *International Journal of Solids and Structures*, 58:106–116,
391 2015.
- 392 [19] Garrett W. Melenka and Jason P. Carey. Experimental analysis of di-
393 amond and regular tubular braided composites using three-dimensional
394 digital image correlation. *Journal of Composite Materials*, 51(28):3887–
395 3907, 2017.
- 396 [20] SL Phoenix. Mechanical response of a tubular braided cable with an
397 elastic core. *Textile Research Journal*, 48(2):81–91, 1978.

- 398 [21] Jitendra S Tate, Ajit D Kelkar, and John D Whitcomb. Effect of braid
399 angle on fatigue performance of biaxial braided composites. *International*
400 *journal of fatigue*, 28(10):1239–1247, 2006.
- 401 [22] Rotich K Gideon, Baozhong Sun, and Bohong Gu. Mechanical behav-
402 iors of four-step 1×1 braided carbon/epoxy three-dimensional com-
403 posite tubes under axial compression loading. *Polymer Composites*,
404 37(11):3210–3218, 2016.
- 405 [23] Duchamp Boris, Legrand Xavier, and Soulat Damien. The tensile be-
406 haviour of biaxial and triaxial braided fabrics. *Journal of Industrial*
407 *Textiles*, 47(8):2184–2204, 2018.
- 408 [24] R Böhm, A Hornig, J Luft, M Becker, I Koch, B Grüber, and W Hufen-
409 bach. Experimental investigation of the strain rate dependent behaviour
410 of 2d biaxially and triaxially reinforced braided composites. *Applied*
411 *Composite Materials*, 21(2):285–299, 2014.
- 412 [25] Anne-Marie Harte and Norman A. Fleck. On the mechanics of braided
413 composites in tension. *European Journal of Mechanics - A/Solids*,
414 19(2):259 – 275, 2000.
- 415 [26] Haili Zhou, Wei Zhang, Tao Liu, Bohong Gu, and Baozhong Sun. Finite
416 element analyses on transverse impact behaviors of 3D circular braided
417 composite tubes with different braiding angles. *Composites Part A:*
418 *Applied Science and Manufacturing*, 79:52–62, 2015.
- 419 [27] Sree Shankhachur Roy, Prasad Potluri, and Constantinos Soutis. Tensile
420 Response of Hoop Reinforced Multiaxially Braided Thin Wall Composite
421 Tubes. *Applied Composite Materials*, 24(2):397–416, 2017.
- 422 [28] Benjamin KO Cheung and Jason P Carey. Improving two-dimensional
423 braided composite tensile properties by including low angle yarn twist:
424 Production, experimental verification, and modeling. *Journal of Engi-*
425 *neered Fibers and Fabrics*, 15:1558925020946449, 2020.

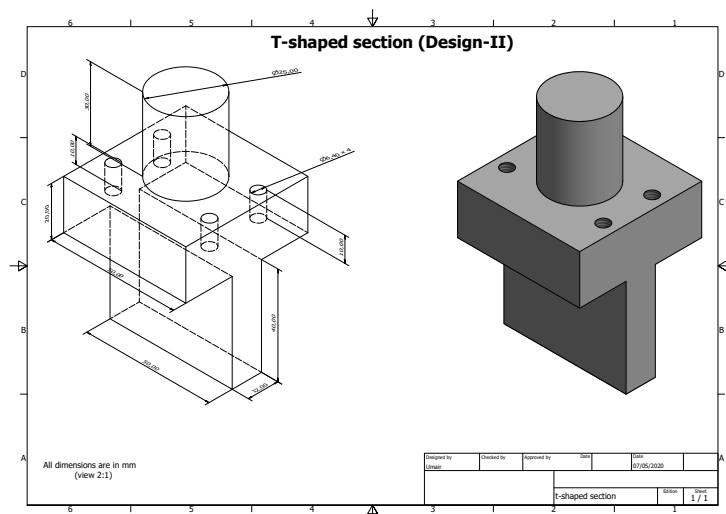
- 426 [29] Othman Laban, Samer Gowid, Elsadig Mahdi, and Farayi Musharavati.
427 Experimental investigation and artificial intelligence-based modeling of
428 the residual impact damage effect on the crashworthiness of braided
429 Carbon/Kevlar tubes. *Composite Structures*, 243:112247, 2020.
- 430 [30] P.B. Ataabadi, D. Karagiozova, M.H. Shaterzadeh, and M. Alves. De-
431 riving unidirectional lamina properties from testing on cylindrical lami-
432 nated specimens. *Composite Structures*, page 112382, 2020.
- 433 [31] Corin Reuter, Kim-Henning Sauerland, and Thomas Tröster. Experi-
434 mental and numerical crushing analysis of circular CFRP tubes under
435 axial impact loading. *Composite Structures*, 174:33 – 44, 2017.
- 436 [32] Yoshito Ikarashi, Toshio Ogasawara, and Takuya Aoki. Effects of cyclic
437 tensile loading on the rupture behavior of orthogonal 3-D woven SiC
438 fiber/SiC matrix composites at elevated temperatures in air. *Journal of*
439 *the European Ceramic Society*, 39(4):806 – 812, 2019.
- 440 [33] Shibo Yan, Xuesen Zeng, and Andrew Long. Effect of fibre architecture
441 on tensile pull-off behaviour of 3D woven composite T-joints. *Composite*
442 *Structures*, 242:112194, 2020.
- 443 [34] G Perillo and AT Echtermeyer. Mode I fracture toughness testing of
444 composite pipes. *Applied Composite Materials*, 20(6):1135–1146, 2013.
- 445 [35] Giovanni Perillo, Robin Vacher, Frode Grytten, Steinar Sørbø, and Vir-
446 gile Delhay. Material characterisation and failure envelope evaluation
447 of filament wound GFRP and CFRP composite tubes. *Polymer testing*,
448 40:54–62, 2014.
- 449 [36] Burgman packings ltd, <https://www.burgmannpackings.com>, accessed
450 on 02-02-2020.
- 451 [37] Easy composites ltd, <https://www.composites.co.uk>, accessed on 01-
452 05-2020.

- 453 [38] Standard test method for transverse tensile properties of hoop wound
454 polymer matrix composite cylinders. ASTM D5450, American Society
455 for Testing and Materials, West Conshohocken, PA, May 2012.
- 456 [39] Standard test method for compressive properties of rigid plastics. ASTM
457 D695 - 02, American Society for Testing and Materials, West Con-
458 shohocken, PA, May 2002.
- 459 [40] Tatiana Stefanov, Bernard Ryan, Alojz Ivanković, and Neal Murphy.
460 Mechanical bulk properties and fracture toughness of composite-to-
461 composite joints of an elastomer-toughened ethyl cyanoacrylate adhe-
462 sive. *International Journal of Adhesion and Adhesives*, 68:142 – 155,
463 2016.
- 464 [41] Abaqus. *ABAQUS/Standard User's Manual, Version 6.14-1, Dassault*
465 *Systèmes*.
- 466 [42] Y. Shi, T. Swait, and C. Soutis. Modelling damage evolution in compos-
467 ite laminates subjected to low velocity impact. *Composite Structures*,
468 94(9):2902–2913, 2012.

469 8 Appendix A: Dimensions of the gripping
 470 fixtures (Design II)



(a) Side fixtures.



(b) T-shaped section.

Figure 15: Technical drawing of the gripping fixtures used for the tensile testing of braided tubes (Design II).